Supporting Information file for:
Simultaneous dual-wavelength source Raman spectroscopy with a handheld confocal probe for analysis of the chemical composition of *in vivo* human skin

Yi Qi[1], Ruochong Zhang[1], Poongkulali Rajarahm[1], Shuyan Zhang[1], Amalina Binte Ebrahim Attia[1], Renzhe Bi[1,*] ,And Malini OLIVO[1]

[1]Institute of Bioengineering & Bioimaging, A*STAR, Singapore 138667, Singapore;

*Corresponding author: Renzhe Bi

Email: Bi_renzhe@ibb.a-star.edu.sg

Table of Content

Section I. Experimental workflow

In this section, we describe the detailed workflow of the experimental setup. The illustration of the workflow is shown in Figure. S1. The left diagram shows the decomposition elements, which include the probe, a huge water droplet, a skin adhesive, a transparent film, and a tiny water droplet. With this workflow and our innovative handheld probe, the confocal Raman measurement can be acquired at any part of body with high efficiency and low cost. During the measurement, after placing the skin adhesive on the skin, the three joints of the mechanical arm are unlocked, and the protruding end of the probe is placed on the skin (e.g. cheek) of the subject. In order to counter the problem of the mechanical arm movement when locking the arm in place, the adhesive has a protruding reservoir, and the probe has a protruding end. This configuration enables users to easily place the probe at the desired location without much hassle. The frame structure of the hollow protrusion enables sufficient space for the filling of the huge water droplet with a syringe and needle. After the huge water droplet fills the reservoir of the skin adhesive, the objective lens can be moved closer to the reservoir for contact with the water. Although this configuration makes the probe stable and robust, since water is directly placed on the skin for a substantial amount of time, the water peak in the acquired Raman data is significantly higher with long-time imaging, interfering with the water content signal of the skin since it is a significant parameter for skin healthy evaluation.

Through iterative experiments and testing, a tiny droplet of water of about 10 μL will be placed instead of placing a huge droplet of water directly on the skin. Such a small amount of water will not interfere the water content of the skin for the duration of the measurement. A thin transparent film will be placed on top of this tiny droplet to isolate the huge water droplet in the skin adhesive. The tiny droplet couples the transparent film to the skin, removing any air gaps in between them, while the huge droplet couples the transparent film to the objective lens when the objective lens moves close to the transparent film. These additional steps not only eliminate the water issue but also stabilizes the skin during imaging. Furthermore, it is also used as a guide to locate the surface of the skin. The portfolios of the working configuration are shown in the right diagram in Figure. S1.

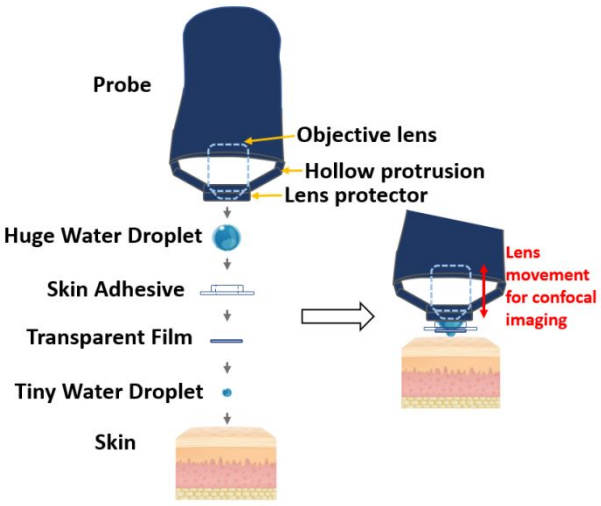

Figure. S1. The workflow and configuration of the human skin inspection with the handheld confocal Raman probe

Section II. The derivation process of the PRSSA in a dual-wavelength excitation Raman spectrometer

From the definition of the Maximum a posteriori probability (MAP) estimate[1, 2], if let f be the sampling distribution of the observation x, θ is an unobserved parameter that needs to be determined, the maximum likelihood estimate (MLE) of θ will be:

$$\hat{\theta}_{MLE}(x) = \arg\max_{\theta} f(x \mid \theta) \tag{1}$$

If we can get a prior distribution g over θ exists, the posteriori distribution of θ can be calculated by using Bayes' theory:

$$f(\theta \mid x) = \frac{f(x \mid \theta) g(\theta)}{\int_{\Theta} f(x \mid \vartheta) g(\vartheta) d\vartheta} \tag{2}$$

Where g is the density function of θ, Θ is the domain of g. Therefore, same as the MLE function, the MAP estimates of θ is:

$$\begin{aligned} \hat{\theta}_{MAP}(x) &= \arg\max_{\theta} f(\theta \mid x) \\ &= \arg\max_{\theta} \frac{f(x \mid \theta) g(\theta)}{\int_{\Theta} f(x \mid \theta) g(\vartheta) d\vartheta} \\ &= \arg\max_{\theta} f(x \mid \theta) g(\theta) \end{aligned} \tag{3}$$

Obviously, the separation of the combined Raman spectrum can meet the requirement of the MAP. The unobserved parameter θ is the spectra that was separated from the dual-wavelength excitation result, while the prior distribution g are premeasurement results with dual-wavelength excitation, laser 1 excitation, and laser 2 excitation. The sampling distribution $f(x \mid \theta)$ is the dual-wavelength excitation result of each experimental measurement.

As mentioned in manuscript section 2.4, here we will describe the derivation process of the PRSSA. The PRSSA is set up depending on some prior hypotheses:

(i) if vector $\boldsymbol{A}$ is combined by vector $\boldsymbol{B}$ and $\boldsymbol{C}$, then:

$$\boldsymbol{A} = \boldsymbol{B} + \boldsymbol{C};$$

(ii) Feature peaks of $\boldsymbol{B}$ and $\boldsymbol{C}$ are fixed, positions and shapes of these feature peaks will not change for the same species sample. The only difference between different samples is the peak intensities of these feature peaks.

(iii) Main peaks (highest intensity) positions in $\boldsymbol{B}$ and $\boldsymbol{C}$ are not overlapped.

Once the combined spectrum and individual spectra meet these requirements, the extraction process of $\boldsymbol{B}$ and $\boldsymbol{C}$ from $\boldsymbol{A}$ can be described as below:

While we want to extract $\boldsymbol{B}'[n,1]$ and $\boldsymbol{C}'[n,1]$ from a combined signal $\boldsymbol{A}'[n,1]$, we must have a group of reference signals as the prior distribution:

$$\boldsymbol{A}[n,1] = \boldsymbol{B}[n,1] + \boldsymbol{C}[n,1] \tag{4}$$

Where $\boldsymbol{A}$ = $[a_1, a_2, a_3, \mathsf{L}\ , a_n]$, $\boldsymbol{B}$ = $[b_1, b_2, b_3, \mathsf{L}\ , b_n]$, and $\boldsymbol{C}$ = $[c_1, c_2, c_3, \mathsf{L}\ , c_n]$. Therefore, from eq. (4):

$$\begin{aligned} a_1 &= b_1 + c_1; \\ a_2 &= b_2 + c_2; \\ &\mathsf{M} \\ a_n &= b_n + c_n; \end{aligned} \tag{5}$$

Therefore, when we have a new combined signal $\boldsymbol{A}'$, which has n components $[a_1', a_2', a_3', \mathsf{L}\ , a_n']$, we can get a similar equation with eq. (4):

$$\boldsymbol{A}'[n,1] = \boldsymbol{B}'[n,1] + \boldsymbol{C}'[n,1] \tag{6}$$

Same as eq. (5), we can get a new group of equations:

$$\begin{aligned} a_1' &= b_1' + c_1'; \\ a_2' &= b_2' + c_2'; \\ &\mathsf{M} \\ a_n' &= b_n' + c_n'; \end{aligned} \tag{7}$$

Since $\boldsymbol{A}, \boldsymbol{B}, \boldsymbol{C},$ and $\boldsymbol{A}'$ are known, we can get the difference $\boldsymbol{X}_A$ between $\boldsymbol{A}$ and $\boldsymbol{A}'$:

$$\boldsymbol{X}_A = \boldsymbol{A}' - \boldsymbol{A} \tag{8}$$

If we separate $\boldsymbol{X}_A$ into two parts: $\boldsymbol{X}_B$ and $\boldsymbol{X}_C$, which stand for the difference between $\boldsymbol{B}$ and $\boldsymbol{B}'$, $\boldsymbol{C}$ and $\boldsymbol{C}'$. Two unknown quantities can be expressed by:

$$\begin{aligned} \boldsymbol{B}' &= \boldsymbol{B} + \boldsymbol{X}_B \\ \boldsymbol{C}' &= \boldsymbol{C} + \boldsymbol{X}_C \end{aligned} \tag{9}$$

Where $\boldsymbol{X}_B + \boldsymbol{X}_C = \boldsymbol{X}_A$, in this equation, $\boldsymbol{X}_B$ and $\boldsymbol{X}_C$ can be also expressed by a proportion of $\boldsymbol{X}_A$:

$$\begin{aligned} \boldsymbol{X}_B &= \boldsymbol{W}_B \times \boldsymbol{X}_A \\ \boldsymbol{X}_C &= \boldsymbol{W}_C \times \boldsymbol{X}_A \end{aligned} \tag{10}$$

Hence, from the eq. (8), (9) and (10) can get:

$$\begin{aligned} \boldsymbol{B}' &= \boldsymbol{B} + \boldsymbol{X}_{\boldsymbol{B}} = \boldsymbol{B} + \boldsymbol{W}_{\boldsymbol{B}} \times \boldsymbol{X}_{\boldsymbol{A}} = \boldsymbol{B} + \boldsymbol{W}_{\boldsymbol{B}} \times (\boldsymbol{A}' - \boldsymbol{A}) \\ \boldsymbol{C}' &= \boldsymbol{C} + \boldsymbol{X}_{\boldsymbol{C}} = \boldsymbol{C} + \boldsymbol{W}_{\boldsymbol{C}} \times \boldsymbol{X}_{\boldsymbol{A}} = \boldsymbol{C} + \boldsymbol{W}_{\boldsymbol{C}} \times (\boldsymbol{A}' - \boldsymbol{A}) \\ & (\boldsymbol{W}_{\boldsymbol{B}} + \boldsymbol{W}_{\boldsymbol{C}} = 1) \end{aligned} \tag{11}$$

In the ideal case, peaks in $\boldsymbol{B}$ and $\boldsymbol{C}$ are not overlapped, so the weightage $\boldsymbol{W}_{\boldsymbol{B}}$ and $\boldsymbol{W}_{\boldsymbol{C}}$ can be determined from the prior distribution:

$$\begin{aligned} \boldsymbol{W}_{\boldsymbol{B}} &= \frac{\boldsymbol{B}}{\boldsymbol{A}} \\ \boldsymbol{W}_{\boldsymbol{C}} &= \frac{\boldsymbol{C}}{\boldsymbol{A}} \end{aligned} \tag{12}$$

However, in the real case, peak values a_n at position n of $\boldsymbol{A}$ normally depends on both b_n of $\boldsymbol{B}$ and c_n of $\boldsymbol{C}$. Meanwhile, these peaks are normally distributed follows the normal distribution, thus, if the center and the width of each peak is prior known, the weightage $\boldsymbol{W}_{\boldsymbol{B}}$ and $\boldsymbol{W}_{\boldsymbol{C}}$ can be determined by MAP estimate. Fortunately, these prior data can be pre-measured with the proposed dual-wavelength excitation Raman system. From the reference results $\boldsymbol{A}$, $\boldsymbol{B}$, $\boldsymbol{C}$, the center position of each peak μ_A, μ_B, μ_C, and the variance of each peak $\sigma^2{}_A$, $\sigma^2{}_B$, $\sigma^2{}_C$ can be determined. The probability density function of each peak in the dual-wavelength excitation reference signal $\boldsymbol{A}$ is:

$$f_A(x_A) = \frac{1}{\sigma_A \sqrt{2\pi}} e^{-\frac{1}{2}(\frac{x_A - \mu_A}{\sigma_A})^2} \tag{13}$$

While it can be combined by the probability density function of $\boldsymbol{B}$ and $\boldsymbol{C}$:

$$\begin{aligned} f_A(x_A) &= f_B(x_A) + f_C(x_A) \\ &= \frac{1}{\sigma_B \sqrt{2\pi}} e^{-\frac{1}{2}(\frac{x_A - \mu_B}{\sigma_B})^2} + \frac{1}{\sigma_C \sqrt{2\pi}} e^{-\frac{1}{2}(\frac{x_A - \mu_C}{\sigma_B})^2} \end{aligned} \tag{14}$$

In the experimental measurement results, due to the peak center and the peak width will not change (prior hypotheses ii), we only need to find out the value of each peak, which is equivalent to find the weightage $\boldsymbol{W}_{\boldsymbol{B}}$ and $\boldsymbol{W}_{\boldsymbol{C}}$ in equation (11). Thus, while b_n ? c_n or c_n ? b_n (prior hypotheses iii), elements w_{b_n} in $\boldsymbol{W}_{\boldsymbol{B}}$ and w_{c_n} in $\boldsymbol{W}_{\boldsymbol{C}}$ will become:

$$\begin{aligned} w_{b_n} &= \frac{b_n}{a_n} \pm w_n \\ w_{c_n} &= \frac{c_n}{a_n} \mp w_n \end{aligned} \tag{15}$$

Where w_n is the weightage coefficient of $\boldsymbol{B}$ at position n, $0 \le w_n \le \frac{c_n}{a_n}$, it depends on the prior distribution of the sample, different category of objects will change the value of w_n. Here, we give an empirical formula for human skin of w_n:

$$w_n = \frac{b_n c_n}{a_n^2} \tag{16}$$

Therefore, while $b_n > 5c_n$:

$$\begin{aligned} b_n^{'} &= b_n + (\frac{b_n}{a_n} + \frac{b_n c_n}{a_n^2})(a_n^{'} - a_n) \\ c_n^{'} &= c_n + (\frac{c_n}{a_n} - \frac{b_n c_n}{a_n^2})(a_n^{'} - a_n) \end{aligned} \tag{17}$$

While $c_n > 5b_n$:

$$\begin{aligned} b_n^{'} &= b_n + (\frac{b_n}{a_n} - \frac{b_n c_n}{a_n^2})(a_n^{'} - a_n) \\ c_n^{'} &= c_n + (\frac{c_n}{a_n} + \frac{b_n c_n}{a_n^2})(a_n^{'} - a_n) \end{aligned} \tag{18}$$

In other situations:

$$\begin{aligned} b_n^{'} &= b_n + (\frac{b_n}{a_n})(a_n^{'} - a_n) \\ c_n^{'} &= c_n + (\frac{c_n}{a_n})(a_n^{'} - a_n) \end{aligned} \tag{19}$$

Where a_n, b_n, c_n and $a_n^{'}$ are the value of $\boldsymbol{A}, \boldsymbol{B}, \boldsymbol{C}$ and $\boldsymbol{A'}$ at position n, while $b_n^{'}$ and $c_n^{'}$ are the value of the extraction result of $\boldsymbol{B'}$ and $\boldsymbol{C'}$ at position n.

Section III. Phantom experiment with Acetic Acid and Ethanol Mixture

Here, Figure. S2 shows the dual-wavelength excitation results of pure acetic acid and ethanol solutions to determine feature peaks for their mixture solutions. Although acetic acid and ethanol have some high peaks, such as the 671 nm excitation peak at around 851 nm and the 785 nm excitation peak at around 859 nm, these peaks are overlapped, which cannot be used as marks to determine the concentration of acetic acid or ethanol in a mixture solution. Therefore, we chose some lower but not overlapped peaks as the feature peaks. As shown in

Figure. S2 (a), the feature peaks of acetic acid only can be found in the 785 nm excitation result due to the 671 nm excitation result only having one distinct peak at 852 nm whereas the 671 nm excitation result of ethanol also has some peaks at this wavelength. Ethanol has more feature peaks in both 671 nm and 785 nm excitation results, so we choose two peaks from each wavelength.

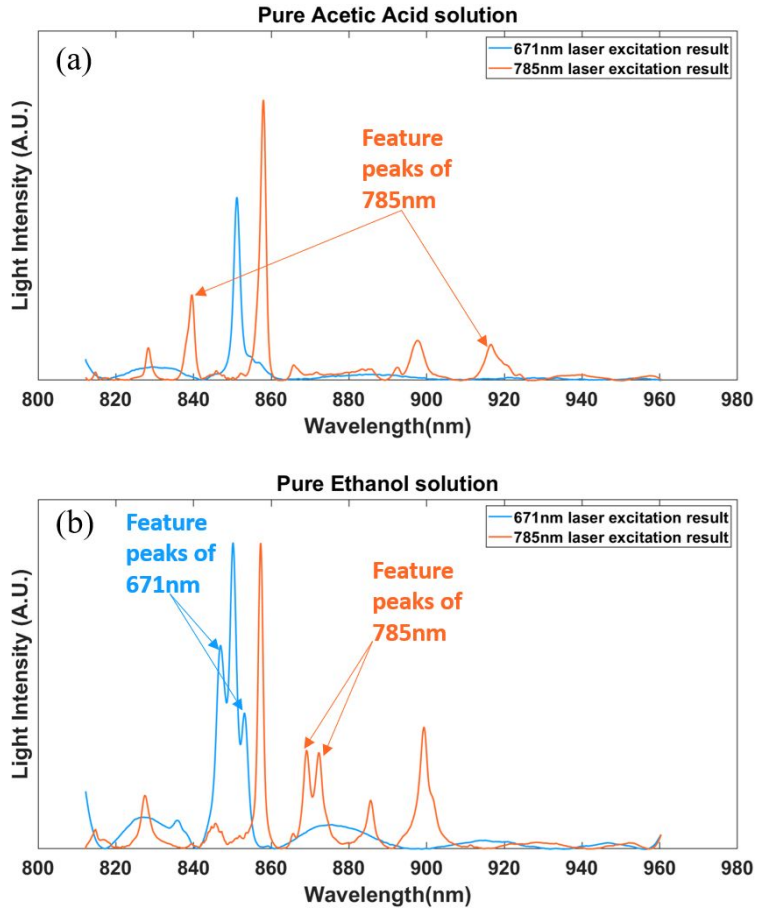

Figure. S2. (a) The feature peaks of pure acetic acid solution in785nm laser excitation result, (b) the feature peaks of pure ethanol solution in 671nm and 785nm laser excitation results.

Figure. S3 shows the extracted FP and HW results with the comparison of the single wavelength excitation results of the mixture of 800 μl ethanol with 100 to 1000 μl acetic acid. The feature peaks of ethanol become lower with the increasing of the concentration of acetic acid, while the feature peaks of acetic acid at 840nm and 918nm become clear.

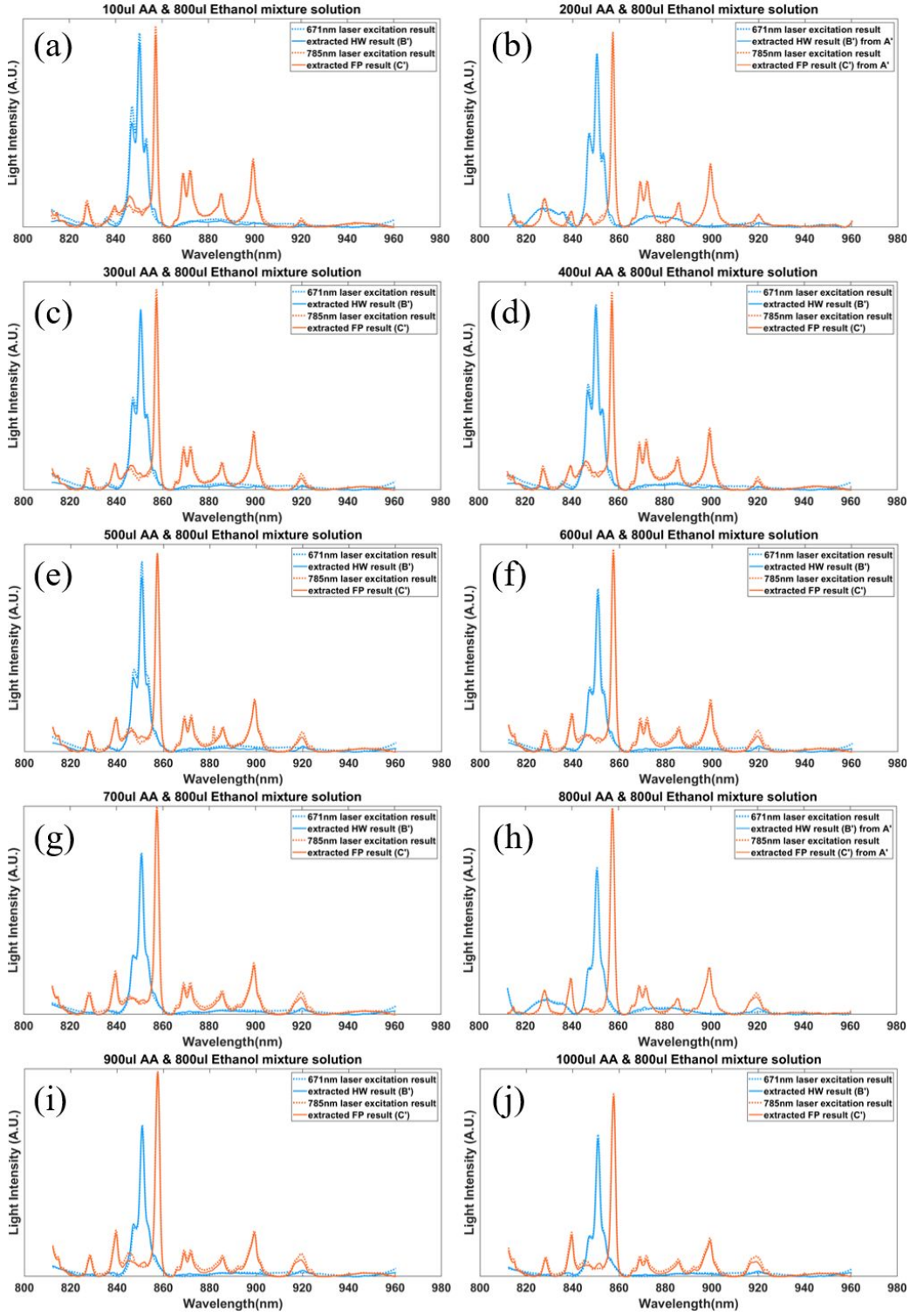

Figure. S3. The Raman spectra with 671nm and 785nm laser excitation and the extracted FP/HW results from the dual-wavelength excitation Raman spectra (a) 100 μL AA and 800

μL Ethanol mixture solution, (b) 200 μL AA and 800 μL Ethanol mixture solution, (c) 300 μL AA and 800 μL Ethanol mixture solution, (d) 400 μL AA and 800 μL Ethanol mixture solution, (e) 5500 μL AA and 800 μL Ethanol mixture solution, (f) 6600 μL AA and 800 μL Ethanol mixture solution, (g) 7700 μL AA and 800 μL Ethanol mixture solution, (h) 800 μL AA and 800 μL Ethanol mixture solution, (i) 900 μL AA and 800 μL Ethanol mixture solution, and (j) 1000 μL AA and 800 μL Ethanol mixture solution.

References

1. D. M. Greig, B. T. Porteous, and A. H. Seheult, "Exact Maximum A Posteriori Estimation for Binary Images," Journal of the Royal Statistical Society: Series B (Methodological) 51, 271-279 (1989).
2. E. Levitan, and G. T. Herman, "A Maximum a Posteriori Probability Expectation Maximization Algorithm for Image Reconstruction in Emission Tomography," IEEE Transactions on Medical Imaging 6, 185-192 (1987).